J|A|C|S ARTICLES

Published on Web 02/10/2009

# Liquid Crystalline Phase Transition Induces Spin Crossover in a Polyelectrolyte Amphiphile Complex

Yves Bodenthin,[†,‡] Guntram Schwarz,[*,§,||] Zbigniew Tomkowicz,[⊥,#] Thomas Geue,[▽] Wolfgang Haase,[⊥] Ullrich Pietsch,[†] and Dirk G. Kurth[§,||,○]

*University Siegen, FB7 Solid State Physics, D-57068 Siegen, Germany, Swiss Light Source, Paul Scherrer Institute, CH-5232 Villigen-PSI, Switzerland, Max Planck Institute of Colloids and Interfaces, D-14424 Potsdam, Germany, Chemische Technologie der Materialsynthese, University Würzburg, D-97070 Würzburg, Germany, Institute of Physical Chemistry, Darmstadt University of Technology, Petersenstrasse 20, D-64287, Germany, Institute of Physics, Jagellonian University, Reymonta 4, 30-059 Kraków, Poland, Laboratory for Neutron Scattering, ETH Zurich and Paul Scherrer Institute, CH-5232 Villigen, Switzerland, and National Institute for Materials Science, 1-1 Namiki, Tsukuba, Ibaraki 305-0044 (Japan)*

Received October 21, 2008; E-mail: guntram.schwarz@matsyn.uni-wuerzburg.de

***Abstract:*** Self-assembly of $Fe^{2+}$ or $Ni^{2+}$ ions and the ditopic ligand 6,6′,6″-bis(2-pyridyl)-2,2′:4′,4″:2″,2‴-quaterpyridine (btpy) through coordinative binding results in rodlike metallosupramolecular coordination polyelectrolytes (Fe-MEPE or Ni-MEPE). Sequential self-assembly with dihexadecyl phosphate (DHP) via electrostatic interactions between MEPE and DHP leads to the corresponding polyelectrolyte amphiphile complex (PAC) with liquid crystalline properties. The MEPE rods are embedded in between the interdigitated DHP layers. Upon heating above room temperature, the Fe-PAC shows an irreversible spin-crossover (SCO) from a diamagnetic low-spin (LS) to a paramagnetic high-spin (HS) state accompanied by a color change from dark blue to pale blue. The SCO is nearly complete (95%) and directly associated with the structure changes induced by the melting of the amphiphilic matrix. The original Fe-PAC architecture does not reassemble upon cooling and remains in a disordered frozen HS state. However, dissolving the heated PAC induces reassembly, and the original dark blue, diamagnetic, ordered material is completely recovered. In comparison to Fe-PAC, Ni-PAC shows the same lamellar structure and the same temperature depended structure changes but has a constant magnetic moment. In contrast to Fe-PAC, in neat Fe-MEPE the SCO depends on the history of the sample and in particular on the amount of included solvent as thermogravimetric analysis, differential scanning calorimetry (DSC), and magnetic measurements indicate. Solid MEPE does not have liquid crystalline properties, and, therefore, the induced structure changes upon heating are constrained by the solid-state architecture, and thus, the SCO in Fe-MEPE is incomplete.

## Introduction

Spin transitions can occur in solids, liquid crystals, and complexes in solution and are generally molecular processes, driven by the entropy gain on going from the low-spin (LS) to the high-spin (HS) state.[1−5] Usually, temperature-driven spin transitions are classified into a discontinuous type, in which the spin state conversion is accompanied by a thermal hysteresis and into a continuous type, where the conversion takes place without hysteresis. In many cases, the discontinuous type is accompanied by a structural change and can be well described by thermodynamics.[6] The structural phase transition is a consequence of the spin transition, or both are coupled to each other.[7] Cooperative effects result in a thermal hysteresis and confer a memory effect on the system. The presence of two different stable electronic or magnetic states within a certain temperature range plays a central role for the development of storage media for signal processing[8] and transduction.[9] Linear spin transition polymers with tightly coupled metal ions, such

[†] University Siegen.
[‡] Swiss Light Source.
[§] Max Planck Institute of Colloids and Interfaces.
[||] University Würzburg.
[⊥] Darmstadt University of Technology.
[#] Jagellonian University.
[▽] Laboratory for Neutron Scattering, ETH Zurich and Paul Scherrer Institute.
[○] National Institute for Materials Science.

(1) Gütlich, P.; Goodwin, H. A. *Spin Crossover in Transition Metal Compounds*; Springer: Verlag, 2004; Vol. 233, pp234−235.
(2) Galyametdinov, Y.; Ksenofontov, V.; Prosvirin, A.; Ovchinnikov, I.; Ivanova, G.; Gütlich, P.; Haase, W. *Angew. Chem., Int. Ed. Engl.* **2001**, *40*, 4269–4271.
(3) van Koningsbruggen, P. J.; Garcia, Y.; Kahn, O.; Fournès, L.; Kooijman, H.; Spek, A. L.; Haasnoot, J. G.; Moscovici, J.; Provost, K.; Michalowicz, A.; Renz, F.; Gütlich, P. *Inorg. Chem.* **2000**, *39*, 1891–1900.
(4) Breuning, E.; Ruben, M.; Lehn, J.-M.; Renz, F.; Garcia, Y.; Ksenofontov, V.; Gütlich, P.; Wegelius, E.; Rissanen, K. *Angew. Chem., Int. Ed. Engl.* **2000**, *39*, 2504–2507.
(5) Soyer, H.; Dupart, E.; Gómez-García, C. J.; Mingotaud, C.; Delhaès, P. *Adv. Mater.* **1999**, *11*, 382–384.
(6) Chernyshov, D.; Burgi, H.-B.; Hostettler, M.; Tornroos, K. W. *Phys. Rev. B* **2004**, *70*, 094116.
(7) Jeftic, J.; Romstedt, H.; Hauser, A. *J. Phys. Chem. Solids* **1996**, *57*, 1743–1750.
(8) Lehn, J.-M. *Proc. Natl. Acad. Sci. U.S.A.* **2002**, *99*, 4763–4768.
(9) Kahn, O.; Martinez, C. J. *Science* **1998**, *279*, 44–48.

 **10.1021/ja808278s CCC: $40.75** 

as $Fe^{2+}$-triazole (trz) complexes have been proposed as a central design motive to control the cooperative switching in molecular magnetic materials.[9] Such compounds and other $Fe^{2+}$ complexes have thus attracted considerable interest for developing functional materials with unique electronic and magnetic properties.[9,10] Coronado et al. recently applied the reverse micelle technique to fabricate bistable nanoparticles of polymeric $[Fe(Htrz)_2(trz)](BF_4)$.[11] Understanding the design principles in order to tailor the electronic and magnetic properties is therefore a central objective in coordination chemistry and materials science. Self-assembly of molecular units into a well-defined supramolecular architecture offers a particularly efficient route toward such materials. This method provides control of structure and function at all length scales and at each level of the structural hierarchy through the design of the components and the types of interactions involved in each step of the self-assembly algorithm.

In an ideal octahedral ligand field the transition metal 3d states split into degenerated $t_{2g}$ (lower) and $e_g$ (higher) levels. Any distortion of the coordination geometry, e.g., as in the pseudo-octahedral geometry, leads to a further splitting, which implies that the effective energy separation between upper and lower sublevels is reduced. Taking this idea further, a severe distortion can reduce the splitting of the 3d sublevels to such an extent that at the given temperature the spin state of the central metal ion changes from a LS to a HS state.[12] For this type of process we favor to use the term spin crossover (SCO) to draw a clear distinction to the well-established entropy-driven spin transition phenomenon.

A versatile approach toward linear spin transition polymers relies on metallo-supramolecular polyelectrolyte amphiphile complexes (PACs), which are self-assembled from ditopic ligands, metal ions, and amphiphilic molecules. The modularity of this approach provides extensive control of structure and properties from molecular to macroscopic length scales by the judicious choice of ligands, metal ions, amphiphiles, and self-assembly conditions. The SCO is induced by deliberately distorting the coordination geometry of the metal centers through a temperature-induced structural reorganization of the amphiphilic matrix, which embeds the linear rigid-rod-type metallo-supramolecular polyelectrolyte (MEPE).[12] The concept to alter the magnetic properties through a structural pertubation has been known for a long time. Already thirty years ago, Cukauskas et al. showed that the Fe−S distances and therefore the spin state equilibrium in iron(III) dithiocarbamate complexes with $Fe-S_6$ cores reacts extremely sensitive to the inclusion of various solvent molecules in the crystal lattice.[13] Recently, Papankova et al. determined through differential scanning calorimetry (DSC), X-ray diffraction (XRD), and magnetic measurements that the water fraction ($x$) in the $[Fe(2,6\text{-bis(benzimidazol-2-yl)pyridine})_2](BPh_4)_2 \cdot xH_2O$ complexes is responsible for the reversibility of the SCO. The temperature induced loss of crystal water can result in an irreversible distortion of the octahedral $Fe-L_6$ core and, therefore, an irreversible HS state of the $Fe^{2+}$ ion.[14]

The PACs combine liquid crystalline (LC) properties through the high fraction of ordered amphiphiles and SCO properties through the MEPE and are, therefore, a new type of functional metallomesogenes. Seredyuk et al. distinguishes three types of synergies between SCO and LC phase transitions in metallomesogenes.[15] First, systems where the phase transitions are coupled and the structure changes drive the spin-state transition; second, systems where both transitions do not couple but coexist in the same temperature region; third, the systems with independent phase transitions at different temperatures. The concept of a structure-induced SCO in metallomesogenes was adopted by Hayami et al. to achieve a reverse (HS→LS) spin transition with tpy ligands modified by long alkyl chains.[16] In these systems, the melting of the amphiphiles is independent from the observed SCO. Here, the structure change is induced by a yet unknown phenomenon, possibly through packing effects of the lattice. Independently, Rajadurai and co-workers recently presented the spin transition in linear $Fe^{2+}$-tpy-based coordination chains.[17] We demonstrated the concept of structure induced SCO first in Langmuir−Blodgett (LB) multilayers of a PAC self-assembled from 1,4-bis(2,2′:6′,2″-terpyridine-4′-yl)benzene, $Fe^{2+}$, and dihexadecyl phosphate (DHP) with a metal ion to DHP stoichiometry of 1:6. Langmuir−Blodgett (LB) transfers result in a PAC architecture where the amphiphilic molecules are arranged in double layers with opposed alkyl chains. The interstitial space is occupied by the MEPE rods.[18] In contrast, bulk PAC, prepared by precipitation from solution, can be described by alternating layers of interdigitated DHP and MEPE strata.[19] The LB film shows a reversible, partial spin crossover slightly above room temperature, which can be assigned to the melting of the amphiphiles. Now, we present that, unlike the LB multilayer, bulk PAC shows a nearly complete SCO in the temperature range from 363 to 398 K just above the melting temperature of the amphiphilic phase. In contrast, neat MEPE shows only a partial, irreversible SCO, which is associated with a distortion of the polymeric backbone induced by evaporating solvent molecules. The strength of the transition depends on the amount of solvent after the drying process, the solvent type, and on the history of the sample. Our new data supports the hypothesis that the SCO in PACs is associated with structure changes in the embedded metallosupramolecular coordination polyelectrolyte induced by the phase transition in the amphiphilic matrix.

## Results and Discussion

**Structural Characterization.** The PAC used here is prepared by sequential self-assembly of 6,6′,6″-bis(2-pyridyl)-2,2′:4′,4″:2″,2‴-quaterpyridine (btpy), $FeOAc_2$, and DHP, resulting in the PAC as shown in Scheme 1.[20] The compounds are named Fe-MEPE and Fe-PAC. The acetate counterions of Fe-MEPE are qualitatively displaced by the DHP molecules, which is

(10) Halder, G. J.; Kepert, C. J.; Moubaraki, B.; Murray, K. S.; Cashion, J. D. *Science* **2002**, *298*, 1762–1765.
(11) Coronado, E.; Galán-Mascarós, J. R.; Monrabal-Capilla, M.; García-Martínez, J.; Pardo-Ibáñez, P. *Adv. Mater.* **2007**, *19*, 1359–1361.
(12) Bodenthin, Y.; Pietsch, U.; Möhwald, H.; Kurth, D. G. *J. Am. Chem. Soc.* **2005**, *127*, 3110–3114.
(13) Cukauskas, E. J.; Deaver, J., B. S.; Sinn, E. *J. Chem. Phys.* **1977**, *67*, 1257–1266.
(14) Papánková, B.; Vrbová, M.; Boca, R.; Simon, P.; Falk, K.; Miehe, G.; Fuess, H. *J. Therm. Anal. Cal.* **2002**, *67*, 721–731.
(15) Seredyuk, M.; Gaspar, A. B.; Ksenofontov, V.; Galyametdinov, Y.; Kusz, J.; Gütlich, P. *J. Am. Chem. Soc.* **2008**, *130*, 1431–1439.
(16) Hayami, S.; Shigeyoshi, Y.; Akita, M.; Inoue, K.; Kato, K.; Osaka, K.; Takata, M.; Kawajiri, R.; Mitani, T.; Maeda, Y. *Angew. Chem., Int. Ed. Engl.* **2005**, *44*, 4899–4903.
(17) Rajadurai, C.; Fuhr, O.; Kruk, R.; Ghafari, M.; Hahn, H.; Ruben, M. *Chem. Commun.* **2007**, 2636–2638.
(18) Bodenthin, Y.; Pietsch, U.; Grenzer, J.; Geue, T.; Möhwald, H.; Kurth, D. G. *J. Phys. Chem. B* **2005**, *109*, 12795–12799.
(19) Meister, A.; Förster, G.; Thünemann, A. F.; Kurth, D. G. *Chem. Phys. Chem.* **2003**, *4*, 1095–1100.
(20) Kurth, D. G.; Lehmann, P.; Schütte, M. *Proc. Natl. Acad. Sci. U.S.A.* **2000**, *97*, 5704–5707.

***Scheme 1.*** Sequential Self-Assembly of btpy, $Fe^{2+}$ Ions, and DHP Results in the MEPE and the Corresponding PAC

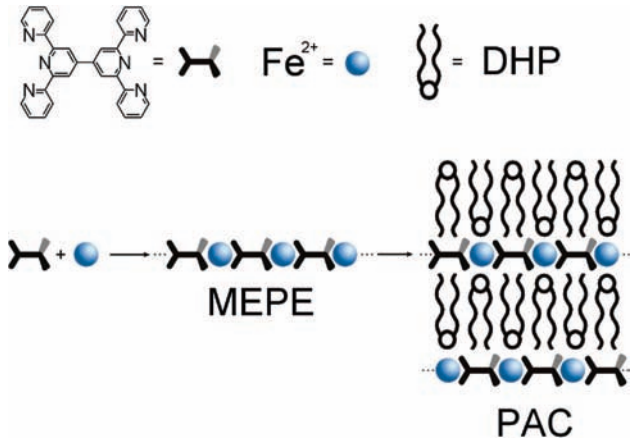


confirmed by NMR and IR measurements.[21] The counterion exchange results in a neutral, hydrophobic assembly that is only soluble in organic solvents like toluene or $CHCl_3$ while Fe-MEPE is soluble in $H_2O$. The stoichiometry is adjusted by the experimental conditions to two DHP molecules per $Fe^{2+}$ ion, which is confirmed by elemental analysis. The dark blue color of Fe-PAC is attributed to the metal to ligand charge transfer (MLCT) band located at 635 nm. This band and the $\pi-\pi^*$ transitions of the coordinating ligand at 294 and 330 nm are characteristic for $[Fe(tpy)_2]^{2+}$ complexes with pseudo-octahedral coordination geometry.[22,23] The transition at 288 nm corresponds to the free ligand and shifts to 294 nm upon metal ion coordination. The absorption at 330 nm appears upon metal ion coordination and is a measure for the number of coordinated tpy-ligand sites.

DSC measurements of neat Fe-MEPE do not show a phase transition in a temperature range from 253 to 453 K. Neat DHP has a unique melting point at 349 K. We determined a transition enthalpy of 119.8 kJ $mol^{-1}$ caused by the melting of DHP, which is in agreement with literature data.[24] In contrast, Fe-PAC reveals 3 phase transitions with maxima at 321, 349, and 419 K. Integration of the DSC curve over the first two transitions yields an enthalpy of 96.6 kJ $mol^{-1}$ based on the DHP fraction, a value well below that of pure DHP. These results show that the interactions of DHP and Fe-MEPE result in a new material with new properties. We note that thermogravimetric analysis (TGA) shows no evidence for oxidation and decomposition up to 453 K.

To characterize the structure of solid Fe-PAC we use small angle neutron- and X-ray scattering (SANS and SAXS). By combination of both methods we can observe the scattering intensity in a broad $q$ range. SANS measurements in the region of $1 \times 10^{-4}$ Å$^{-1} \leq q \leq 0.22$ Å$^{-1}$ show one scattering peak at $q = 0.2$ Å$^{-1}$ with the corresponding spacing of $d = 32$ Å.[25] The angle-dispersive SAXS spectrum of Fe-PAC (Figure 1)

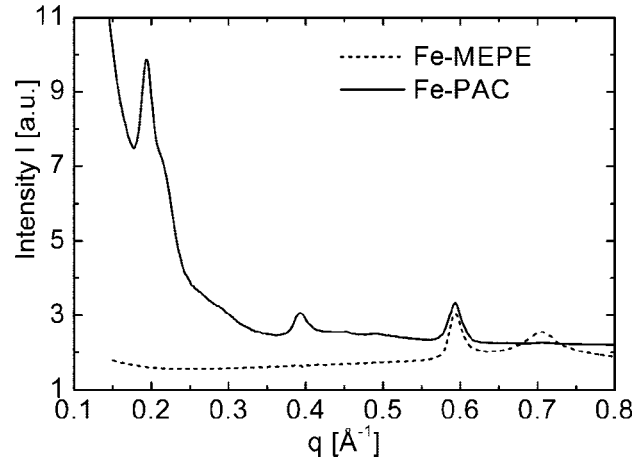


***Figure 1.*** SAXS intensity ($I$) of Fe-MEPE (dotted line) and Fe-PAC (solid line) as a function of the transfer momentum ($q$) at room temperature. For Fe-PAC the peaks occur at q values of 0.2, 0.39, and 0.59 Å$^{-1}$. The Fe-MEPE sample shows two peaks at $q = 0.59$ and 0.71 Å$^{-1}$ corresponding to the Fe−Fe-distance of 10.7 Å and the average thickness of a MEPE rod, $d \approx 9$ Å, respectively.

shows three equidistant peaks at $q = 0.2$, 0.39, and 0.59 Å$^{-1}$. All-*trans*-DHP has a length of approximately 23 Å, and the Fe-MEPE rods have an average diameter of approximately 10 Å.[19] If we assume interdigitated DHP molecules plus a MEPE layer we expect a periodicity of 33 Å for a single layer (Scheme 1). This distance is close to the experimental determined value of 32 Å ($q = 0.2$ Å$^{-1}$). The absence of a peak at $q = 0.11$ Å$^{-1}$ and other higher order peaks at lower $q$ values proves that there is no DHP double-layer structure, as observed in the corresponding LB multilayers,[12] and that the peak at $q = 0.2$ Å$^{-1}$ is the first order peak of a single layer structure. Figure 1 also shows the X-ray scattering data (dotted line) of neat Fe-MEPE with peaks at $q = 0.59$ Å$^{-1}$ and $q = 0.71$ Å$^{-1}$. We assign the peak at $q = 0.59$ Å$^{-1}$ to the Fe−Fe distance ($d = 10.7$ Å) of the coordination polymer. The second peak at $q = 0.71$ Å$^{-1}$ corresponds to a periodicity of 9 Å and is assigned to the average Fe-MEPE rod diameter, with 12 Å being the largest and 6 Å being the smallest dimension of the ligand, respectively. Now, the DHP length of 23 Å and the experimental determined MEPE thickness of 9 Å lead to a single layer thickness of 32 Å in agreement with the SAXS and SANS data. We note that the peak at $q = 0.59$ Å$^{-1}$ for the MEPE repeat unit (Fe−Fe distance $d = 10.7$ Å) in the MEPE scattering curve occurs at the same position as the third order lamellar structure peak measured in the PAC spectrum (see below). WAXS measurements of Fe-PAC show a single peak at $q = 1.52$ Å$^{-1}$, which indicates a hexagonal packing of the alkyl chains in the amphiphilic matrix with a Bragg spacing of 4.1 Å. In a single undistorted hexagonal packing mode only one peak is observable because the (100) and (010) reflections coincide. The peak can be assigned to a 2D hexagonal alkyl chain lattice described by an orthorhombic subcell (SC) with the length $a_{SC} = 4.80$ Å, $b_{SC} = 8.32$ Å, and the angles $\alpha_{SC} = \beta_{SC} = \gamma_{SC} = 90°$.[19] The setting angle $\tau$ (angle between the carbon backbone and $a_{SC}$) is 60°. By use of this subcell an average spatial requirement of one alkyl chain is calculated to be 20 Å$^2$. In summary, our analysis shows that the Fe-PAC can be best described as liquid crystalline material with layers of close packed interdigitated amphiphiles while the interstitial space between the amphiphile layers is occupied by the oppositely charge MEPE rods.

(21) Lehmann, P.; Symietz, C.; Brezesinski, G.; Krass, H.; Kurth, D. G. *Langmuir* **2005**, *21*, 5901–5906.
(22) Schütte, M.; Kurth, D. G.; Linford, M. R.; Cölfen, H.; Möhwald, H. *Angew. Chem., Int. Ed. Engl.* **1998**, *37*, 2891–2893.
(23) Constable, E. C.; Thompson, A. M. W. C. *J. Chem. Soc., Dalton Trans.* **1992**, 2947–2950.
(24) Thünemann, A. F.; Kurth, D. G.; Beinhoff, M.; Bienert, R.; Schulz, B. *Langmuir* **2006**, *22*, 5856–5861.
(25) The momentum transfer $q$ is defind as $q = 2\pi E/hc \sin 2\theta$, where $2\theta$ is the scattering angle, $E$ the energy, and $h$ and $c$ are Planck's constant and light velocity.

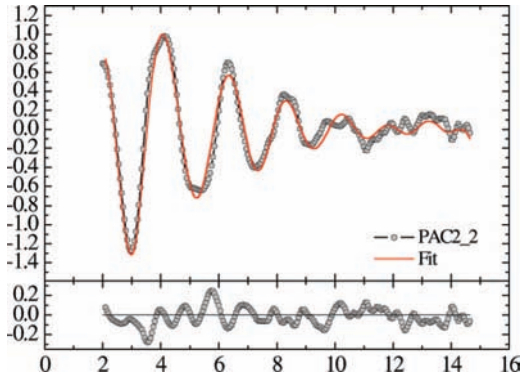


***Figure 2.*** Experimentally determined and calculated EXAFS functions $\chi(k) = (\mu(k) - \mu_0(k))/\mu_0(k)$ of Fe-PAC. $k$ represents the reduced wavenumber $k = \hbar^{-1}(2m_e(E - E_0))^{0.5}$. The best fit of the experimental data is obtained with two different Fe−N distances of $r_1 = 1.885 \pm 1 \times 10^{-2}$ Å and $r_2 = 1.972 \pm 1 \times 10^{-2}$ Å and occupation numbers of 2 and 4, respectively.

The environment of the $Fe^{2+}$ coordination center is explored by X-ray absorption fine structure experiments (EXAFS). Figure 2 shows a representative EXAFS function $\chi_{exp}(k) = (\mu(k) - \mu_0(k))/\mu_0(k)$ of the solid PAC and the best fit using a two-core approximation with two different Fe−N distances ($r_1$ and $r_2$). The central bond length, $r_1$, amounts to $1.885 \pm 1 \times 10^{-2}$ Å, and the peripheral bond length, $r_2$, to $1.972 \pm 1 \times 10^{-2}$ Å, respectively. The occupation numbers amount to 2 for the central positions and 4 for the distal positions in agreement with a pseudo-octahedral coordination geometry. The values corresponds fairly well with average Fe−N next-neighbor distances found in the single crystal structure of the mononuclear $[Fe(tpy)_2]^{2+}$ complex.[26] For $Fe^{2+}$ complexes these length values are typical for a low spin state of the metal ion. Finally, it should be noted that it is not possible to obtain a satisfactory fit with a single shell model, where all bond distances are equal (not shown). The coordination geometry around the $Fe^{2+}$ ions is pseudo-octahedral, which is generally observed with tpy ligands.[27]

DSC measurements show that the phase transition at 321 K is reversible. Upon further heating, two nonreversible transitions appear at 349 and 420 K (Figure 3). To explore the origin of the transitions revealed by DSC, we take a detailed look at the structure using temperature dependent energy-dispersive SAXS. This technique provides good counting statistics in a $q$ range from $q = 0.05$ to 1.0 $Å^{-1}$ and a time resolution of one minute per spectra.[28] Figure 3 summarizes the collected SAXS pattern for one heating cycle and the DSC measured heat flow as a function of temperature. The peak at $q = 0.14$ $Å^{-1}$, which is present over the entire temperature range, is associated with the K fluorescence of the $Fe^{2+}$ ions at $E = 6.4$ keV.[29] The stack-of-layers superstructure of PAC leads to the above-mentioned scattering peaks at $q = 0.2$, 0.39, and 0.59 $Å^{-1}$, corresponding to the first-, second-, and third-order scattering peak corresponding to a translational period of $d = 32$ Å. As discussed above, the intensity at $q = 0.59$ $Å^{-1}$ has two contributions, one from the lamellar superstructure and one from the MEPE-repeat unit.

At 315 K the first ($q = 0.2$ $Å^{-1}$) and second ($q = 0.39$ $Å^{-1}$) order scattering peaks begin to shift toward lower $q$ values, finally reaching values of $q = 0.18$ and 0.37 $Å^{-1}$, respectively. The intensity of the second-order peak becomes considerably smaller. The lamellar layer thickness increases to $d = 35$ Å. Upon heating only the peak intensity associated with the lamellar structure decreases while the peak for the Fe−Fe distance remains mainly unaffected. This structure change coincides with the loss of order between the alkyl chains starting at 321 K as indicated by a decrease of the corresponding WAXS peak (not shown). We note that at this point the lamellar ordering is maintained. According to the WAXS measurements, in the range of the second phase transition measured by DSC (332−388 K), the amphiphiles melt, and the hexagonal order vanish completely. The layer thickness decreases now from $d = 35-33$ Å. The phase transitions are reversible as long as the temperature does not exceed 400 K. If the PAC is heated above 400 K, the first-order scattering peak becomes broad, and an additional peak occurs at $q = 0.26$ $Å^{-1}$, corresponding to a length of 22 Å. Because of the broadness of both scattering peaks it is not possible to separate one from the other (Figure 3). Additionally, a further scattering peak appears at $q = 0.52$ $Å^{-1}$ (second order). The corresponding thickness of 22 Å for this new phase is associated with DHP, which has an estimated length of 23 Å at room temperature. We assume that heating above 410 K induces a phase separation and a complete structural reorganization of the PAC. At temperatures around 395 K, the peak at $q = 0.59$ $Å^{-1}$ becomes more intense, possibly due to annealing effects of the MEPE rods resulting in an increase of ordered domains. Finally, we note that heating the Fe-PAC above 360 K results in an irreversible color change from dark blue to pale blue. The loss of the associated MLCT band corresponds to a change in the electronic configuration of the $[Fe(tpy)_2]^{2+}$ complex, which is associated with the distortion of the coordination geometry. In the next section we are, therefore, going to address the magnetic properties of the Fe-PAC.

**Magnetic Properties.** The structure change of the PAC within the temperature range from 363 to 395 K observed by SAXS is accompanied by a SCO, which is identified by magnetic measurements. In Figure 4 we present the magnetic susceptibility $\chi_M T$ of Fe-PAC as function of temperature. As one can see, $\chi_M T$ increases above 363 K to values of about $\chi_M T = 2.77$ $cm^3$ $mol^{-1}$ K at approximately 395 K, reflecting a spin crossover from a diamagnetic LS state to a paramagnetic HS state of the $Fe^{2+}$ ions (Figure 4 A). The value of $\chi_M T = 2.77$ $cm^3$ $mol^{-1}$ K corresponds to a magnetic moment of 4.7 Bohr magneton per $Fe^{2+}$ ion. Upon further heating up to 460 K, $\chi_M T$ remains constant. The SCO temperature range is estimated to be 363−393 K, and the increase of $\chi_M T$ is most rapid after the melting of the amphiphilic matrix and the corresponding structure change in the layer structure.

In contrast to Fe-PAC, $\chi_M T$ of Fe-MEPE increases slowly but continuously. The SCO in Fe-MEPE is incomplete. The $\chi_M T$ difference for the Fe-MEPE ($\Delta(\chi_M T)_{MEPE}$) in the temperature range from 295 to 395 K is 0.46 $cm^3$ $mol^{-1}$ K in comparison to $\Delta(\chi_M T)_{PAC} = 2.53$ $cm^3$ $mol^{-1}$ K for Fe-PAC. We choose 395 K as the upper temperature value because $\chi_M T$ of the Fe-PAC reaches the maximum value at this temperature. The increase of $\chi_M T$ for this Fe-MEPE sample does not stop immediately with the beginning of cooling, which indicates a nonequilibrium

(26) Baker, A. T.; Goodwin, H. A. *Aust. J. Chem.* **1985**, *38*, 207–214.
(27) Constable, E. C.; Baum, G.; Bill, E.; Dyson, R.; Eldik, R. v.; Fenske, D.; Kaderli, S.; Morris, D.; Neubrand, A.; Neuburger, M.; Smith, D. R.; Wieghardt, K.; Zehnder, M.; Zuberbühler, A. D. *Chem.−Eur. J.* **1999**, *5*, 498–508.
(28) Bodenthin, Y.; Grenzer, J.; Lauter, R.; Pietsch, U.; Lehmann, P.; Kurth, D. G.; Möhwald, H. *J. Synchrotron Rad.* **2002**, *9*, 206–209.
(29) Henke, B. L.; Gullikson, E. M.; Davis, J. C. *At. Data Nucl. Data Tables* **1993**, *54*, 181–342.

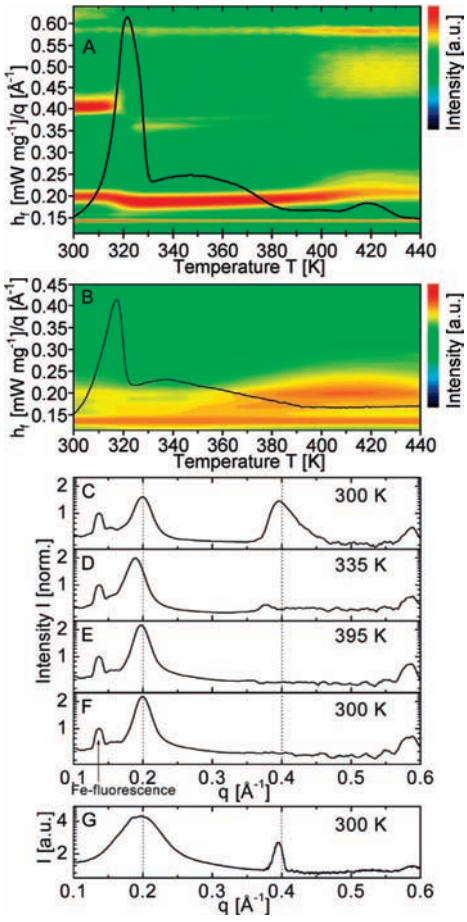


***Figure 3.*** Time-resolved energy-dispersive SAXS (EDR) pattern of Fe-PAC (A) and Ni-PAC (B). The scattering intensity is color coded as indicated on the right side, with dark blue for the lowest and red for the highest intensity. The solid line shows the corresponding heat flow ($h_f$) measured by DSC as function of temperature. Notably, the heat flow $h_f$ and the transfer momentum ($q$) of the EDR measurement share the same ordinate axis. (A) EDR of Fe-PAC in the $q$ range from 0.05 to 0.8 Å$^{-1}$ collected with two detectors (detector D1, $0.05 \leq q \leq 0.35$ Å$^{-1}$; detector D2, $0.33 \leq q \leq 0.80$ Å$^{-1}$). The two peaks at $q \approx 0.14$ Å$^{-1}$ (orange/red) and 0.16 Å$^{-1}$ (yellow) persistent over the whole temperature range correspond to the iron $K_\alpha$ and $K_\beta$ fluorescence at 6.4 and 7.1 keV. Between 318 and 330 K the first- and second-order peaks at $q = 0.2$ and 0.4 Å$^{-1}$ shift to lower $q$ values (bold red lines) indicating the rearrangement of the PAC layer structure, which is also detected by DSC (black line). Above 330 K the amphiphiles begin to melt, indicated by the loss of the WAXS peak (not shown). During the second transition observed by DSC in the temperature range of 330−385 K, the $q$ values of the first- and second-order scattering peaks shift from 0.17 to 0.19 Å$^{-1}$ and 0.35 to 0.38 Å$^{-1}$, respectively (see C−F). (B) The main part of the Ni-PAC scattering curve detected by D1 with an effective range of $0.05 \leq q \leq 0.28$ Å$^{-1}$. The line at $q \approx 0.13$ Å$^{-1}$ (orange/red) persistent over the whole temperature range corresponds to the $K_\alpha$ nickel fluorescence at 7.5 keV. Similar to A, the first order peak at $q = 0.2$ Å$^{-1}$ shifts to lower $q$ values during the rearrangement of the layer structure and shifts back to the original value after the melting transition of the amphiphiles. (C−F) The line scans at different temperatures extracted from the Fe-PAC SAXS pattern are shown in C−F. Scan C is at 300 K before heating, D at 335 K where the first and second order peaks shift to lower $q$ values (to $q = 0.17$ Å$^{-1}$ and $q = 0.37$ Å$^{-1}$, respectively) due to the melting of the amphiphiles. Scan E shows the scattering intensity close to the end of SCO at 395 K. The first-order peak is shifted back to $q = 0.19$ Å$^{-1}$, and the second order peak vanishes. This structure remains stable upon cooling back to 300 K (F). The peak at 0.59 Å$^{-1}$ is assigned to the Fe−Fe-distance. G show the scattering intensity ($I$) as a function of $q$ from an angle dispersive measurement of Ni-PAC at room temperature. The scattering peak values and, therefore, the lamellar structure is similar to Fe-PAC at the same temperature (C).

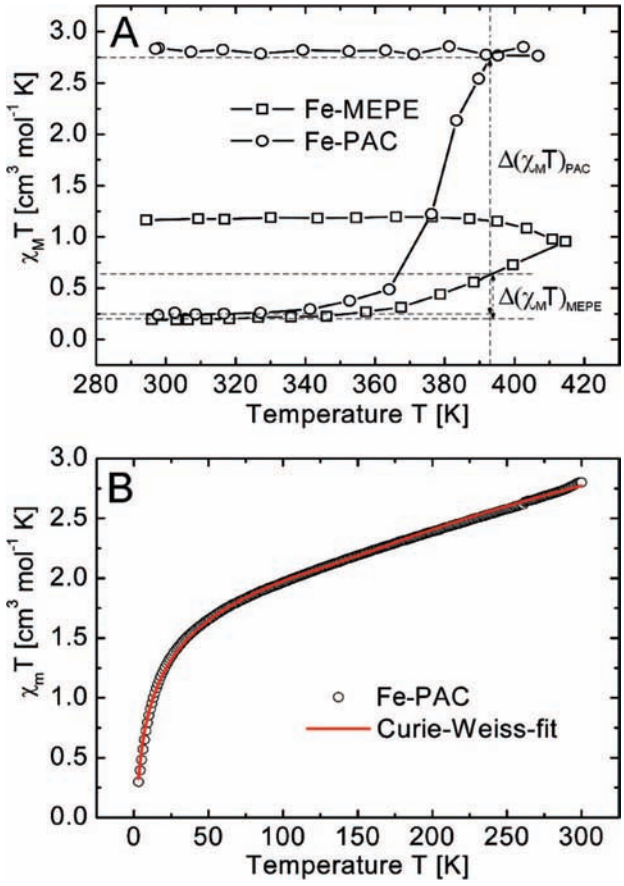


***Figure 4.*** (A) High-temperature part of $\chi_M T$ as a function of temperature of Fe-MEPE and Fe-PAC during a first heating−cooling cycle. The data, taken with a Faraday balance, reveals an increase of the magnetic susceptibility of the two samples starting nearly at the same temperature. This corresponds to a spin crossover between a diamagnetic LS state and a paramagnetic HS state of the $Fe^{2+}$ ions. At 395 K the transition of Fe-PAC is nearly complete, $\Delta(\chi_M T)_{PAC}$ is 2.53 cm$^3$ mol$^{-1}$ K but for Fe-MEPE $\Delta(\chi_M T)_{MEPE}$ is only 0.46 cm$^3$ mol$^{-1}$ K. The HS state is permanent. (B) Magnetic susceptibility, $\chi_M T$, as a function of temperatures from 300 to 4 K. The red line is the fit of $\chi_M T$ to the Curie−Weiss law. The data was taken using a SQUID magnetometer after heating the sample above the SCO temperature to switch the $Fe^{2+}$ ions into the HS state.

situation where the high temperature state has not yet been completely developed before cooling has started (vide infra).

The HS state of Fe-MEPE and Fe-PAC remains stable upon cooling. We note that magnetic response of Fe-MEPE depends on the preparation of the sample. The MEPE samples are prepared in acetic acid because the ligand is soluble in acetic acid. The acid is evaporated under ambient conditions, and the solid MEPE is dried for 24 h under high vacuum. DSC of a so-handled solid sample, denoted as Fe-MEPE-HOAc, shows a broad transition with a maximum at 386 K, which is close to the boiling point of acetic acid (391 K) (Figure 5B). If solid Fe-MEPE-HOAc is dissolved in water and evaporated and dried as described above, the resulting Fe-MEPE-$H_2O$ sample shows a DSC transition with a maximum at 363 K, which is close to the boiling point of water (371 K) (Figure 5A). The evaporated solvent fraction can be measured through themogravimetric analysis (TGA). At 400 K the mass change due to the loss of HOAc (6.4%) or $H_2O$ (5.8%) is nearly identical. As expected, vaccuum-dried Fe-PAC does not show a mass loss up to 460 K (Figure 5C).

The $\Delta(\chi_M T)$ values at room temperature before and after heating for Fe-MEPE-$H_2O$ and Fe-MEPE-HOAc are 0.85 and

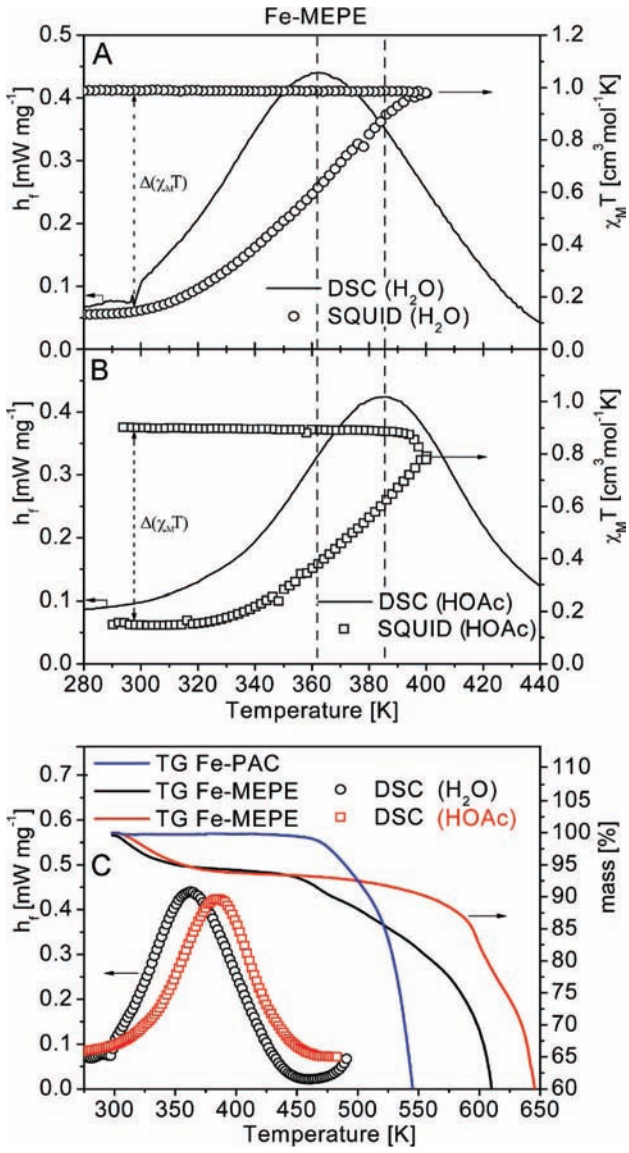


***Figure 5.*** (A and B) Heat flow ($h_f$) measured by DSC and the product of magnetic susceptibility ($\chi_M$) and temperature ($T$) measured by SQUID as a function of temperature of Fe-MEPE prepared from $H_2O$ (A) and HOAc (B). The transition maxima of Fe-MEPE-$H_2O$ (363 K) and Fe-MEPE-HOAc (386 K) are marked with dotted lines. The transition temperatures correlate with the boiling points of the solvents used for the preparation of the Fe-MEPE samples. (C) Heat flow ($h_f$) measured by DSC for Fe-MEPE-$H_2O$ (black circles) and Fe-MEPE-HOAc (red squares) and the mass of Fe-PAC (blue line), Fe-MEPE-$H_2O$ (black line) and Fe-MEPE-HOAc (red line) measured by TGA as a function of temperature.

0.74 $cm^3$ $mol^{-1}$ K, respectively (Figure 5). The corresponding $\chi_M T$ values at room temperature after heating are 0.99 and 0.89 $cm^3$ $mol^{-1}$ K for Fe-MEPE-$H_2O$ and Fe-MEPE-HOAc, respectively. We note that $\chi_M T$ of the Fe-MEPE-HOAc sample continues to increase as the sample is cooled. At 400 K $\chi_M T$ is 0.77 $cm^3$ $mol^{-1}$ K and increases to 0.89 $cm^3$ $mol^{-1}$ K during cooling, similar to the Faraday measurement shown in Figure 4A. On the other hand the $\chi_M T$ value of 0.99 $cm^3$ $mol^{-1}$ K at 400 K of the Fe-MEPE-$H_2O$ sample remains constant upon cooling. TGA measurements suggest that the equilibration of Fe-MEPE-HOAc takes up to 30 min at 380 K, after this time the mass loss discontinues. Likewise, magnetic measurements with the Faraday balance at the same temperature indicate a constant $\chi_M T$ value after 30 min (not shown). These results

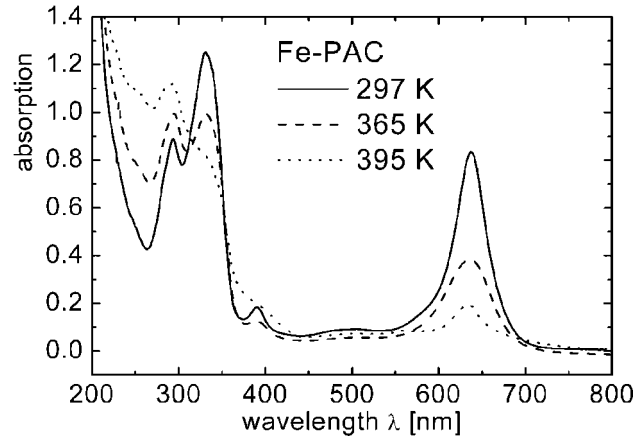


***Figure 6.*** UV−vis spectra of Fe-PAC, deposited on quartz glass, at three different temperatures. At room temperature (solid line) the spectrum shows the absorption bands for free tpy ligand at 294 nm, coordinated tpy ligand at 330 nm, a weak d−d transition at 392 nm, and the characteristic MLCT transition at 635 nm (black line). At 365 K, just above the SCO temperature of 363 K, the MLCT transition has decreased by approximately 50% indicating a change in the coordination geometry and the electronic state of the central $Fe^{2+}$ ions (dashed line). At 396 K the band at 325 nm decreases to the same extend as the band at 293 nm increases due to the changes in the PAC structure (dotted lines).

demonstrate that the magnetic response of Fe-MEPE depends on the preparation conditions.

Coming back to Fe-PAC, we note that the magnetic moment of 4.7 $\mu_B/Fe^{2+}$ at $T = 395$ K indicates that most $Fe^{2+}$ ions participate in the SCO. Assuming pure spin magnetism, the magnetic moment of free $Fe^{2+}$ is estimated to be 4.9 $\mu_B/Fe^{2+}$. This value can be considered as a lower limit, e.g., Constable et al. determined 5.3 $\mu_B/Fe^{2+}$ for mononuclear $[Fe(tpy)_2]^{2+}$ complexes ($g = 2.16$).[27] Apparently, nearly all metal ions in the PAC sample change their spin state, indicating that the coordination geometry of the central $Fe^{2+}$ ions has been sufficiently distorted. At this point, the assembly is presumably kinetically trapped or frozen, and therefore, the SCO is irreversible giving rise to a permanent HS state. The SCO is also confirmed by a change in color (vide supra). The UV−vis spectra of Fe-PAC, recorded on dried thin film samples on quartz glass, show no change in the temperature range from 298 to 363 K. Heating the films above 363 K results in an intensity decrease of the MLCT band and of the band at 330 nm, indicating a change in the electronic state, that is in the coordination geometry of the metal ion. Simultaneously, the band at 294 nm, corresponding to free tpy ligand, increases (Figure 6), suggesting at least partial disassembly of the MEPE backbone. At 395 K the MLCT band does not decrease any further in intensity. The spectra do not change upon cooling the sample to 298 K, which is in agreement with the magnetic measurements discussed in the previous section. We note that the structural, magnetic, and optical properties are completely recovered if the PAC is dissolved in $CHCl_3$ and isolated as solid powder as in the synthesis of the original material. This observation confirms our hypothesis that heating changes the supramolecular architecture and results in a kinetically trapped state. In the bulk, the amphiphiles, ligands, and metal ions cannot reassemble upon cooling and, therefore, the SCO is irreversible. To confirm this hypothesis, we performed the following control experiment. We replaced $Fe^{2+}$ by $Ni^{2+}$ and prepared the Ni-PAC sample in the exact same way as the previously analyzed sample. The $Ni^{2+}$ ion has an electronic configuration of $3d^8$ that is $t_{2g}^6e_g^2$ in case of an octahedral geometry. SAXS and WAXS

measurements demonstrate that Ni-PAC is isostructural to Fe-PAC (Figure 3G). Under the same conditions and with the same measuring techniques as for Fe-PAC, we find that heating Ni-PAC induces almost identical changes of the supramolecular architecture (Figure 3A and B). First, we note the same shift of the first order scattering peak from $q = 0.2$ to 0.17 $Å^{-1}$ in the range from 315 to 326 K as in the case of Fe-PAC due to a rearrangement in the amphiphilic matrix. Second, we observe an increase of $q$ from $q = 0.17$ to 0.2 $Å^{-1}$ with the beginning of the amphiphile melting from 330 to 395 K. The structure changes in the range of 300−400 K cause the above-mentioned heat flow. However, since Ni-MEPE does not show a SCO, the structural change in this temperature range is not associated with the SCO. The measured magnetic moment remains constant at 3.0 $\mu_B/Ni^{2+}$ in the temperature range from 273 to 450 K, which is in good agreement with the theoretical value for pure spin magnetism of 2.9 $\mu_B/Ni^{2+}$. Comparing the data for MEPE, Fe-PAC and Ni-PAC, we can conclude that the amphiphilic phase transition and the SCO are coupled in such a way, that the melting of the amphiphilic matrix induced the SCO. Furthermore, we can exclude that the SCO is caused by a chemical reaction involving the metal ions, ligands or amphiphiles.

Figure 4B shows the low temperature part of the magnetic susceptibility, $\chi_M T$, of Fe-PAC measured from 300 to 2 K after the sample was heated to 395 K and cooled back down to room temperature. Fitting the $\chi_M T$ data to the Curie−Weiss law reveals information about the magnetic moment carried by the metal centers at room temperature and possible magnetic ordering schemes (Figure 4B, red line). We find a negative Weiss constant of $\Theta = -36.6$ K $\pm$ 0.6 K indicating an antiferromagnetic coupling between the $Fe^{2+}$ centers at very low temperatures as it was already proved for the MEPE based on the same btpy ligand and the 4f metal ion $Yb^{2+}$.[30] Furthermore, we determine a magnetic moment of 4.6 $\pm$ 0.2 $\mu_B/Fe^{2+}$ from the fit, which is in good agreement with the Faraday balance results discussed above (Figure 5A). The same data is obtained if the sample is now heated from 2 K up to room temperature or if the temperature is sweep back and forth. This observation confirms the persistence of the HS state down to low temperatures. For this particular material, therefore, it is not possible to determine if there is a thermal hysteresis in the classical sense because the HS state is a kinetically trapped or frozen.

## Summary and Conclusion

Sequential self-assembly of $Fe^{2+}$ or $Ni^{2+}$ with ditopic bisterpyridines and DHP results in a PAC with a lamellar architecture. The DHP forms interdigitated monolayers with hexagonal order and a layer thickness of 23 Å. The interstitial space is filled with MEPE, which is formed by metal ion induced self-assembly of the transition metal ions and the ditopic ligands. EXAFS of the Fe-PAC sample shows that at room temperature the coordination environment of the metal centers is pseudo octahedral with two different Fe−N distances $r_1 = 1.86$ Å and $r_2 = 1.97$ Å, respectively. At the same temperature magnetic measurements using SQUID and Faraday balance reveal that only a minor part of the $Fe^{2+}$ ions (15%) are in the HS state. Heating the Ni- or Fe-PAC samples causes melting of the amphiphiles and a loss of order in the amphiphilic matrix. Above 400 K we observe an irreversible phase transition and a corresponding loss of order of the lamellar architecture. The structure change is accompanied by a (irreversible) color loss from dark blue to pale blue. The Fe-PAC shows an irreversible SCO in the temperature range from 363 to 395 K. It is easy to envision that the SCO properties such as the transition temperature or the thermal hysteresis can be affected by the design of the components and the supramolecular architecture.

Here, we provide further evidence that melting of the amphiphilic phase in Fe-PAC effects the spin state of the embedded Fe-MEPE. The liquid crystal phase transition causes sufficient strain, which results in a distortion of the embedded metallosupramolecular coordination polyelectrolyte. In case of bulk Fe-PAC, the SCO is close to quantitative. UV−vis data supports the hypothesis that the polymeric backbone is severely distorted indicated by the decrease of the MLCT band intensity and an increase of the band of free, uncoordinated tpy ligand. The irreversible thermochromism, which is associated with the SCO, could be employed as tag to indicate a temperature threshold, e.g., in food safety. Likewise, the magnetic response of neat MEPE is susceptible to the inclusion of solvent molecules in the lattice. The spin transition in Fe-MEPE is rationalized by a distortion of the coordination geometry through a contraction of the lattice as the solvent molecules evaporate. The SCO in Fe-MEPE is, however, only partial due to the packing constraints in the solid.

Further support for our hypothesis is provided by a comparison of LB films and bulk PAC. In LB films, melting of the amphiphilic matrix causes a reversible but partial spin crossover slightly above room temperature (320 K). In contrast, the bulk Fe-PAC undergoes a nearly complete spin crossover with respect to the $Fe^{2+}$ ions indicating a major structural perturbation of the MEPE. The temperature range of the SCO (363−395 K) is higher than in the LB film suggesting cooperative motions involving the amphiphilic matrix as well as the polymeric backbone. And finally, the HS state is permanent due to a kinetically frozen state. The differences in the magnetic response are attributed to the distinctive structure of thin films compared to bulk samples. Whereas in thin films the PACs are organized in preferentially oriented two-dimensional planes, the bulk phase is most likely composed of randomly oriented domains, which inhibit relaxation upon cooling. If the SCO was driven exclusively by an entropy gain of the spin transition, we would not expect to see such significant differences.

In summary, we document that the magnetic response of PACs can be controlled by the design of the supramolecular architecture at all length scales including constituents, composition, and self-assembly conditions. In the future it will be of interest to study how we can design the magnetic response function, including the temperature range of SCO, reversibility, and thermal hysteresis, through the choice of ligands, amphiphiles, metal ions stoichiometry, and self-assembly conditions in these linear one-dimensional polymer composites.

## Experimental

btpy was synthesized according to a literature procedure.[31] Chemicals were purchased from Aldrich and were used without further purification. A representative example of a MEPE synthesis with a metal ion to ligand ratio of 1:1 is as follows: According to a literature procedure, 25 mg (0.448 mmol) Fe was weighted and dissolved in refluxing glacial acetic acid to produce 77.86 mg (0.448

(30) Carlson, C. N.; Kuehl, C. J.; DaRe, R. E.; Veauthier, J. M.; Schelter, E. J.; Milligan, A. E.; Scott, B. L.; Bauer, E. D.; Thompson, J. D.; Morris, D. E.; John, K. D. *J. Am. Chem. Soc.* **2006**, *128*, 7230–7241.

(31) Constable, E. C.; Cargill Thompson, A. M. W. *J. Chem. Soc., Dalton Trans.* **1992**, 3467–3475.

mmol) of dispersed $Fe(OAc)_2$.[32] After cooling down to room temperature, the dispersion of white $Fe(OAc)_2$ powder is added to 242.01 mg (0.448 mmol) of the ligand dissolved in acetic acid (75 vol %). The solvent is evaporated under ambient pressure and the Fe-MEPE (319.88 mg) is recovered as dark blue solid, which is dried under vacuum. A representative PAC synthesis with a 1:2 stoichiometry of $Fe^{2+}$ to DHP was as follow: 1511.42 mg (0.896 mmol) DHP was added to 319.88 mg Fe-MEPE, and the solids were dispersed in 100 mL of $CHCl_3$. After 24 h stirring at room temperature, the solvent of the clear dark blue solution was evaporated under ambient pressure, and the dark blue solid was dried under vacuum. Thin films on quartz side were prepared by dropping 200 $\mu$L of PAC dissolved in $CH_3Cl$ onto the precleaned quartz slide. Evaporation of the solvent under ambient pressure produced dark blue semitransparent thin films. UV−vis spectra were recorded with a Cary 500i UV−vis-NIR spectrometer. The Fe-PAC showed bands at 290, 330, and 390 nm. The magnetic properties were probed by using a DC-SQUID magnetometer from Quantum Design and a Faraday balance with maximum upper temperatures of 400 and 473 K. The SQUID provides a sensitivity of $10^{-7}$ emu, while for high temperatures we probed the sample by a Faraday balance under He gas atmosphere with a sensitivity of $10^{-6}$ emu (external field $B = 1.2$ T).[33] We used a heating rate of 2 K $min^{-1}$ for the magnetic measurements as well for the structural investigations. DSC and TGA measurements were performed under a $N_2$ atmosphere with a heating rate of 2 K $min^{-1}$ on a DSC 204 F1 Phoenix and a TG 209 F1, respectively. The error for comparison temperatures of different experiments is estimated to be ±5 K. SAXS was performed at the energy-dispersive reflectometer at the BESSY II synchrotron.[34] Here, the hard X-ray decay of a bending magnet is used for scattering providing X-rays in an energy range of 5−25 keV. SAXS patterns are collected as a function of temperature using two energy-dispersive detectors with an energy resolution of $\Delta E/E = 10^{-2}$. To enhance the accessible $q$ range the detectors are equipped at two fixed exit angles of $2\theta = 2.79°$ and $2\theta = 5.78°$ with respect to the incident beam. This geometry provides sufficient counting statistics in a $q$ range of $0.05 \le q \le 0.80$ Å$^{-1}$ and a time resolution of 60s per spectra.[28] SANS were performed on the SANS II beamline at SINQ, Paul Scherrer Institut (PSI), Switzerland. The experiments were carried out with three different geometries using three different wavelengths of $\lambda_{1,2} = 6.73$ Å and $\lambda_3 = 19.6$ Å and three different sample to detector distances of $SDD_1 = 1.2$ m, $SDD_2 = 5$ m, and $SDD_3 = 6$ m.[35] EXAFS experiments were undertaken at the KMC 2 beamline at BESSY II, using the fluorescence yield $I_{fluo}(E) \approx \mu(E)$ of the $Fe^{2+}$ ions, where $\mu(E)$ represents the absorption.[36] To explore the data, we used a simplex fitting algorithm to the EXAFS standard formula $\chi_{sim} = \Sigma_i(N_i/kr^2{}_i) \exp(-2\sigma^2{}_i k^2) \exp(-2r_i/\lambda(k)) \times |f_i(k,r_i)| \sin(2kR_i + \Phi(k,r_i))$ minimizing the residual $S = (\Sigma(\chi_{exp}(k) - \chi_{sim}(k))^2/\Sigma\chi_{exp}{}^2(k))^{0.5}$. $k$ represents the reduced wavenumber $k = \hbar^{-1}(2\mu_e(E - E_0))^{0.5}$, where $E$ is the photon energy, $E_0$ the iron absorption edge, $N_i$ the occupation number, $\sigma^2$ the Debye−Waller factor, and $r_i$ the radius of the shell. The amplitude $f(k,r)$ and phase $\Phi(k,r)$ were calculated with the ab initio FEFF6 calculation.[37] To avoid the "multiple solution trap"[38] the Fe−N distances were restrained to vary in an interval of ±0.2 Å.

**Acknowledgment.** This work was supported by Deutsche Forschungsgemeinschaft as part of the priority program 1137 "Molecular Magnetism". This work is partly based on experiments performed at the Swiss spallation neutron source SINQ, Paul Scherrer Institut, Villigen, Switzerland and on the BESSY II synchrotron Berlin, Germany. The authors thank Helmuth Möhwald for valuable discussions and Martin Lommel for the experimental support.

JA808278S

(32) Hardt, H. D.; Möller, W. *Z. Chem.* **1961**, *313*, 57–59.
(33) Merz, L.; Haase, W. *J. Chem. Soc., Dalton Trans.* **1980**, 875–879.
(34) Pietsch, U.; Grenzer, J.; Geue, T.; Neissendorfer, F.; Brezsesinski, G.; Symietz, C.; Möhwald, H.; Gudat, W. *Nucl. Instrum. Methods Phys. Res., Sect. A* **2001**, *467*, 1077–1080.
(35) Strunz, P.; Mortensen, K.; Janssen, S. *Phys. B* **2004**, *350*, 783–786.
(36) Erko, A.; Packe, I.; Gudat, W.; Abrosimov, N.; Firsov, A. *SPIE* **2000**, *4145*, 122–128.
(37) Rehr, J. J.; Albers, R. C.; Zabinsky, S. I. *Phys. Rev. Lett.* **1992**, *69*, 3397–3400.
(38) Michalowicz, A.; Vlaic, G. *J. Synchrotron Rad.* **1998**, *5*, 1317–1320.